Design and Validation of a Micro-AUV for 3-D Sampling of Coherent Ocean Features

David Heermance[1], Dhanushka Kularatne[2], Jose Daniel Hernandez Sosa[3],
M. Ani Hsieh[2] and Ryan N. Smith[1†]

***Abstract*—The ocean, as vast as it is complex, has a plethora of phenomena that are of legitimate scientific interest, e.g., ocean fronts and Lagrangian Coherent Structures. These coherent ocean features occur from tidal mixing and ocean circulation, and are generally characterized with narrow bands of locally intensive physical gradients with enhanced circulation, biological productivity, and optimal transport phenomena. Spatial extents of these phenomena can be on the order of 10's of km^2, and episodic events can last from hours to weeks. These ocean features are 3-dimensional, where to date, most research has focused on examining only their 2-dimensional expression. These coherent features cannot be thoroughly studied through traditional sampling involving random and/or discrete sampling approaches, moreover it is not cost-effective to validate new sampling methodologies in the field. Additionally, operating a single robotic platform in the ocean is hard, and coordinating a team of robots presents challenges in communication on top of dealing with navigation and complex ocean dynamics.**

To this end, in this paper we present the development and validation of a micro Autonomous Underwater Vehicle for deployment in a laboratory testing tank able to accurately simulate large-scale ocean dynamics. The goal is to provide a laboratory-scale, underwater vehicle for validating and testing algorithms and strategies to sample the 3-dimensional structure that exists in coherent ocean features, e.g., ocean fronts, eddys and Lagrangian Coherent Structures, for the purpose of developing better physical and biological models to aid autonomous ocean research. We provide a detailed description of the vehicle and present multiple results from lab experiments.

I. INTRODUCTION

Geophysical fluid dynamics (GFD) is the study of natural fluid flows that span large physical scales, such as oceans, eddies, jets, the atmosphere, and rivers. Although GFD flows are naturally stochastic and aperiodic, they do exhibit coherent structures. These coherent structures divide broader areas with different water masses, vertical

[1]David Heermance and Ryan N. Smith are with the Department of Physics and Engineering, Fort Lewis College, Durango, CO 81301, USA dheermance7@gmail.com, rnsmith@fortlewis.edu

[2]Dhanushka Kularatne and M. Ani Hsieh are with the SAS Laboratory, Mechanical Engineering & Mechanics Department, Drexel University, Philadelphia, PA 19104, USA {dnk32,mhsieh1}@drexel.edu

[3]Jose Daniel Hernandez Sosa is with ULPGC - Dpto. Informatica y Sistemas, Campus de Tafira, 35017 Las Palmas de G.C., Spain daniel.hernandez@ulpgc.es

[†]Corresponding author.

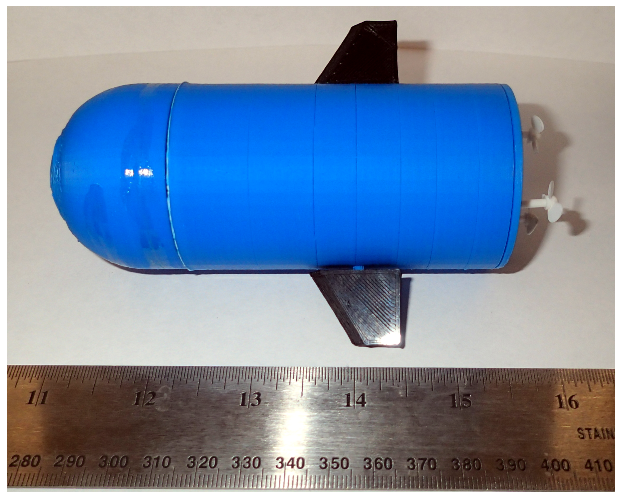

Fig. 1. Images of the micro-AUV designed to gather 3-D data on coherent ocean structures.

structure, or fluid dynamics. A front can be observed or detected via changes in multiple environmental properties (e.g., temperature, nitrate, salinity, etc.) [1]. However, precise study of these features has been a persistent challenge in ocean science as they occur across a variety of spatial scales; along-frontal scales of 1 km to $10,000$ km, cross-frontal scales of 10 m to 100 km, and vertical scales of 10 m to 1000 m. Additionally, ocean fronts vary temporally on scales ranging from a few hours to a few weeks and even longer, e.g., the Kuroshio Front of the eastern coast of Japan. Given these challenges, ocean fronts cannot be studied through conventional oceanographic techniques [2], and a reliable model of the 3-dimensional (3-D) structure and behavior of fronts does not yet exist.

Current characterization and sampling methods for ocean fronts involve heuristics based on ship-based and remotely sensed measurements, e.g., [3]–[5]. These heuristics inform oceanographers for sampling the different water masses that occur across and within the frontal boundaries. This is a difficult task and results in very sparse sampling when conducted from large, manned vessels. To this end, it is of interest to examine the use of autonomous surface and underwater vehicles cooperatively to provide a cost-effective and

978-0-933957-43-5

sustainable approach to sample these dynamic features at high spatial and temporal resolution, for the purpose of developing models, both physical and biological. Additionally, there is also interest to determine the viability of using transport controlling ocean fronts, e.g., Lagragian coherent structures [6], which divide the flow field into dynamically distinct regions, as reduced-order models for predicting ocean dynamics. To develop such models, we must first gather enough information to begin to characterize these dynamic features in the flow field at multiple spatiotemporal scales.

In this paper, we present the development and validation of a micro Autonomous Underwater Vehicle (AUV) (Fig. 1) for deployment in a laboratory testing tank able to accurately simulate large-scale ocean dynamics. The goal is to provide a mechanism for validating and testing algorithms and strategies to sample the 3-D structure that exists in coherent ocean features, e.g., ocean fronts, eddys, and Lagragian Coherent Structures, for the purpose of developing better physical and biological models to aid autonomous ocean research. We provide a detailed description of the vehicle and present results from lab experiments. This innovative micro-AUV will extend current capabilities to the full water column and help develop autonomy to increase our understanding of the 3-D dynamics occurring in GFD and other ocean processes.

Through this work, we aim to overcome theoretical and technical challenges in the development of a general mathematical and control framework for distributed autonomous sensing and tracking of GFD and to understand the utility of GFD with respect to increasing the autonomy of unmanned marine vehicles.

We additionally extend our previous work in [7] and [8] to demonstrate the capabilities of a micro-AUV for adaptive sampling of spatiotemporally dynamic features. The structure of the paper is as follows. We briefly summarize related work in Section II. The design of the vehicle is presented in Section III and the experimental methodology is presented in IV. A summary of the experimental results is presented in Section V. We conclude with a discussion of experimental insights and directions for future work in Section VI.

II. RELATED WORK

Robotic platforms hold the promise of a revolution in ocean sampling. Considerable study has been reported on control design for AUVs for adaptive ocean sampling and coordinated control of multi-vehicle systems, e.g., [9]–[16]. Applications of ocean sampling techniques for AUVs are discussed in [13], [14], [17]–[20], with ocean front perception and detection specifically addressed in [1], [9], [10], [21], [22]. Ocean front detection and characterization has been extensively studied without *in situ* robotics through satellite remote sensing [3], [4], [23], [24]. These algorithms provide the foundation for the heuristics (priors) of robot comprehensible features. Along with steering an AUV to the right locations, research exists in the area of static sensor placement to maximize knowledge return [25].

To address adaptation, researchers have implemented human-in-the-loop solutions; static paths are created and alternative static paths are generated by domain experts after analyzing collected data [26]–[29]. In other cases, path planning techniques are applied to repeatedly generate optimal pre-computed trajectories [30], [31].These methods have their advantages, however we are interested in enabling decision making for path adaptation on-board the vehicle. Some results have implemented information-based metrics and machine learning to optimally determine a path or sensor placement based on reduction of overall covariance of the scalar field in question. Recent work in [9], [10] begins to address the issue of on-board decision making and adaptation, but approaches the problem from a multiple underwater vehicle point-of-view, with constraints on communication among the fleet.

Similar work in cooperative boundary tracking for robotic teams, which relies on one-dimensional parametrization include [32], [33] and [34], [35] for static and time-dependent cases respectively. Formation control strategies for distributed estimation of level surfaces, scalar fields, and transport controlling features in the ocean are presented in [36]–[39]. These works leverage the spatio-temporal sampling capabilities of a team of robots where real-time tracking of ocean frontal features is accomplished by fusing multiple measurements obtained on opposite sides of the front. Different from the aforementioned research efforts, this work focuses on the design and validation of a micro-AUV for adaptive sampling. Here, we enable *in situ* robotic adaptation to environmental conditions for a single vehicle based on real-time measurements for targeted sampling of ocean fronts. Because operation of robots in the ocean is both expensive and time consuming, there is a need to validate algorithms in a controlled laboratory setting before deploying to field tests. Currently, the capability to do this in a laboratory, with AUVs at scale, is nonexistent.

III. VEHICLE DESIGN

The micro-AUV presented in this paper consists of four main aspects; 1) physical design, 2) control, 3) power, and 4) communication. For the physical design of the vehicle for use in the proposed testing environment, decisions were based on scale, feasibility, and functionality. We modeled the vehicle after existing full-scale AUVs, and implemented a design incorporating propeller-driven thrusters, control planes, and sliding masses to obtain full six degree-of-freedom control. Additional consideration was required to ensure the vehicle was water tight. A power source was chosen to allocate an adequate testing time in a small form factor. For communications, we required a method to send data to and from the vehicle in real-time for localization and data collection, as necessary.

A. *Physical Design*

The micro-AUV was designed to mimic a typical torpedo-shaped vehicle, and operate in a 9 m^2 tank. The dimensions of the micro-AUV are approximately 11.5 cm in length and approximately 4.9 cm in diameter. The micro-AUV is shown fully assembled in Fig. 1, and disassembled in Fig. 2. We remark that this is not absolutely to scale for underwater vehicles. The length of the micro-AUV was designed for the experimental environment it was to work in, and the flows created therein. Given the appropriately-scaled length, the diameter was increased to fit all necessary components within the hull. The entire hull and components were designed using the 3-D CAD program SolidWorks, and printed using ABS plastic on a commercial, RepRap 3-D printer. This facilitated rapid prototyping and modifications, as deemed necessary, during the entire design and testing process.

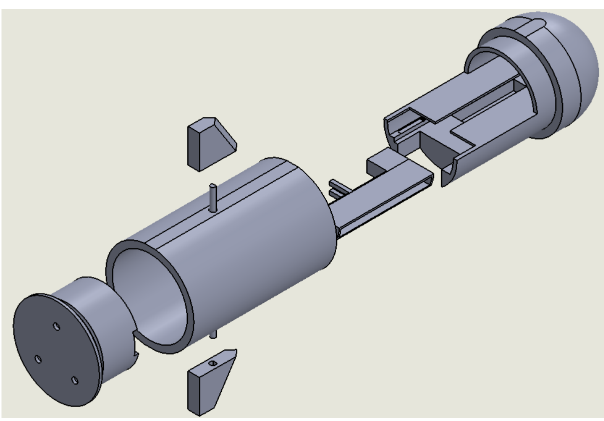

Fig. 2. An exploded view of the micro-AUV.

There are a variety of AUVs on the market, from fixed buoyancy AUV's with propellers, to gliders with a buoyancy engine, to hybrids incorporating aspects of both styles. Due to the small vertical scales the micro-AUV needed to traverse (≈ 0.5 m) the chosen design focused on propellers for propulsion, rather than a buoyancy engine. The micro-AUV was designed to have a fixed buoyancy, and to be slightly positively buoyant, with a mass of 223 g. This enables motion in the z-axis, since the change in pressure within 0.5 m was nearly negligible for our application. To make the micro-AUV nearly neutrally buoyant, lead shot was added to the gaps of the infill pattern during the 3-D printing process. Approximately equal weight was added to both the nose cone and tail cone to keep the vehicle level. This made the micro-AUV initially within 5 g of neutrally buoyant. To ensure water tightness, O-rings were designed around the front edge of the hull, and around the rear cap. Slots were allocated into each part to hold 2.4 mm diameter O-rings, with a $1:5$ ratio of exposed to enclosed material for the seal. Standard O-ring filament was used to create custom O-rings for the seals. To ensure a waterproof seal at locations of hull extrusions, e.g., motors, a silicon dioxide sealant was applied. Finally, the exterior of the micro-AUV was coated with a two-part epoxy to seal any small holes and ensure the ABS plastic did not absorb any water.

B. *Control*

The vehicle is equipped with a custom controller board, which contains a micro-controller, an inertial measurement unit, and a pair of motor controller integrated circuits [**?**]. This board, as well as the communication chip, is located on a shelf in the nose cap to keep it off of the bottom of the micro-AUV. Forward motion is controlled with three independently-operated micro-DC motors [40]. The differential drive configuration, as well as the control model is similar to the ones used in [41]. Yaw is controlled with two control planes attached to an Hitec HS-35HD ultra-nano servo motor [42]. The control planes are attached to a vertical axis which goes through the hull and attaches the nano servo. Pitch is controlled with a sliding mass within the vehicle, attached to another ultra-nano servo motor. This sliding mass was a 3-D printed hollow bar with lead shot placed inside of it. Any shift forward or backward from this neutral position will induce pitch. An annotated view of this part is shown in Fig: 3. The lead shot added into this shifting bar brings the vehicle to nearly neutral buoyancy. The ultra-nano servo motor runs along a notched rail inside the left of the nose cone, below the shelf where the components lay. The teeth were printed on this rail, and act as the rack for this rack and pinion system.

C. *Power*

The micro-AUV is powered by a 3.8V micro lithium-ion battery [43]. The lithium-ion battery was chosen over a lithium-polymer battery due to the energy density, size limitations, and lack of deformation that occurs with use in the lithium-ion. This power source supports approximately 90 minutes of operation and is located inside the bottom of nose cap part, below the shifting mass.

D. *Communications*

One crucial step to reaching full operational functionality was the ability to have real-time communication

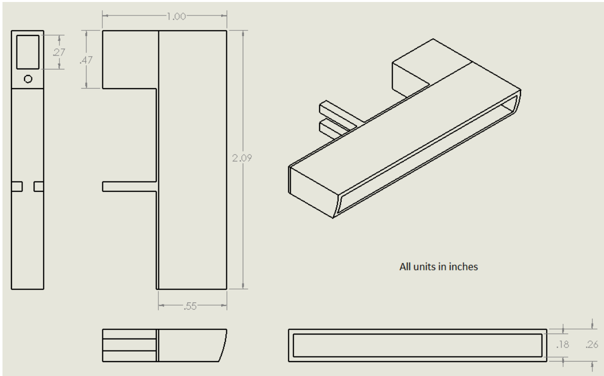

Fig. 3. An annotated view of the sliding mass bar

with the micro-AUV. As this is a testbed platform, we aimed to implement a communication feedback system to enable real-time data transfer and remote control, as necessary. This was facilitated through the use of 900 MHz XBee radio modules [44]. These devices were found to transmit through approximately 1 m of water. Similar 2.4 GHz units were tested, but were unable to penetrate through the water.

IV. EXPERIMENTAL VALIDATION

To evaluate the functionality of the micro-AUV, we implement an adaptive sampling and tracking strategy for time-varying flow fields, i.e., [7], [8]. Tests were conducted in the multi-robot Cohearent Structure Testbed (mCoSTe) [41], [45] at Drexel University. In these experiments, we first verified the water tightness, communication system functionality, and the 2-dimensional (2-D) mobility of the micro-AUV on the water surface in still water. The limitations of the radio communication, and the motion capture system were found to define the dive parameters of the micro-AUV in the mCoSTe. The underwater 3-D functionality of the micro-AUV was validated, as well as the ability to track velocity fronts in time-independent, and time-varying flow fields.

A. Experimental Setup

The experimental setup consists of three major components, the mCoSTe tank, the infrared motion capture camera system, and the PIV/PTV sensors. The mCoSTe is an indoor laboratory experimental test-bed that consists of three experimental flow tanks [41]. We employed one of the mCoSTe's experimental flow tanks, the Multi-Robot (MR) Tank, which is 3 m x 3 m x 1 m. The MR tank is pictured in Fig. 4. The MR tank is able to simulating either time-independent or time varying coherent ocean features to scale. The flows in the tanks are patterned after the wind-driven double gyre flow model which is often used to emulate large-scale recirculation in the ocean [46]. Additional

Fig. 4. Experimental flow tank

details of the various components of the mCoSTe, and flows that can be created, can be found by referring to [41]. Localization of the micro-AUV is provided by an external motion capture system which utilizes infrared reflective particles attached to the exterior of the micro-AUV. A unique pattern of retro-reflective markers were affixed to the vehicle to enable real-time tracking of the vehicles full six-dimensional pose using a network of overhead, infrared-motion capture cameras within the mCoSTe. With the unique patterned of reflectors affixed to the micro-AUV, the orientation, location, and heading of the micro-AUV within the MR tank are registered and recorded.

B. Experimental Methodology

To evaluate the functionality of the micro-AUV, we deploy it into the MR tank. The first set of experiments evaluated the 2-D mobility of the micro-AUV on the surface of the water. General propulsion and maneuverability are tested, followed by execution of traveling to predetermined waypoints. The capabilities of the radio communication and the motion capture system were evaluated to determine the dive parameters for the micro-AUV.

Test 1: Validation of operation of all components and that the hull was watertight.

Test 2: A program to remotely control the micro-AUV was implemented to validate operation of the micro-AUV and all components *in situ*. All of the initial program parameters used are identical to the ones used for the mASV's as in [8].

Test 3: Next, a closed loop control program was implemented to validate the accuracy of the micro-AUV on the surface, as well as the motion capture and communication system.

Test 4: The dive parameters of the micro-AUV were determined through the underwater functionality of the communication system. The mCoSTe was filled up to 0.5 m due to building regulations, and retro-reflective markers are used in conjunction with the camera system above the mCoSTe.

Test 5: To determine 3-D functionality, the remote control program was used to test pitch control underwater, providing motion in the z-axis.

To evaluate the feasibility of the proposed algorithm in tracking velocity fronts for the micro-AUV, we use a variety of tests in the MR tank, similar to those performed in [8]. Since the micro-AUV was not equipped with on-board flow sensing capabilities, artificial sensor outputs were generated to simulate the flow in the tank. This methodology allows us to evaluate the algorithm on various flow fields which are not easily realizable with generated flows in the experimental tank. We considered the following scenarios in our experimental evaluation.

Test 6: A *time-invariant* flow field was considered in which the x component V_x and the y component V_y of the flow velocity at a point (x, y) is given by

$$V_x = \nabla_x \psi \tag{1a}$$
$$V_y = \nabla_y \psi \tag{1b}$$
$$\psi = -\left[y - A\sin\left(\omega_b x\right)\right]^2 \tag{1c}$$

where A is the amplitude of the created front and ω_b is the spacial frequency of the front. The micro-AUV was used to track this simulated front in the MR tank. This is represented in Fig. 5, at $t = 0.0$ s.

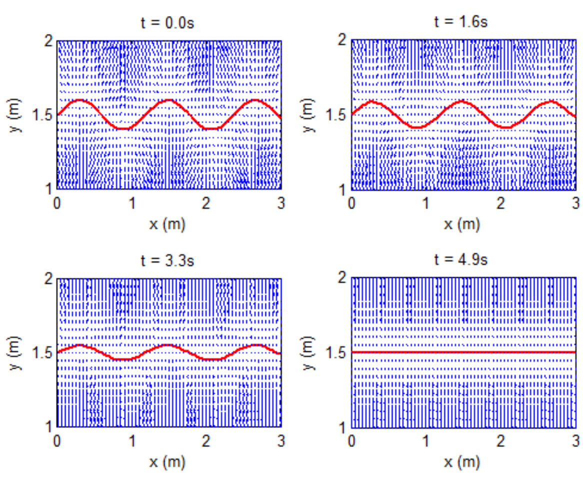

Fig. 5. Time varying velocity front with $A = 0.1$, $\omega_b = \frac{1}{6\pi}$, $\omega_m = \frac{1}{\pi}$ and $I = 0$

Test 7: A *periodic* flow field was considered where the x component V_x and the y component V_y of the flow velocity at a point (x, y) at time t is given by

$$V_x = \nabla_x \psi + \eta_x \tag{2a}$$
$$V_y = \nabla_y \psi + \eta_y \tag{2b}$$
$$\psi = -\left[y - A\cos\left(\omega_m t\right)\sin\left(\omega_b x\right)\right]^2 \tag{2c}$$

Terms in (2) have identical meanings as (1) but with η_x and η_y representing the noise components with standard deviation $\sigma = \sqrt{2I}$ and ω_m representing the temporal frequency of the front created. The underlying flow field with $A = 0.1$, $\omega_b = \frac{1}{6\pi}$, $\omega_m = \frac{1}{\pi}$ and $I = 0$ is shown in Fig. 5

Test 8: Similar to **Test 7**, but with noise intensity I, added to the velocity measurements to simulate measurement noise. I was set to the maximum value used in [8], of $I = 0.05$.

For tests 6-8, we implemented a modification of the algorithm used for adaptive tracking of time varying systems presented in [8]. In summary, the algorithm generates an initial path for the AUV/ASV to traverse the front, based on a prior characterization of the front, see Algorithm 1. This initial path is generated as a zig-zag pattern with a predefined swath width. The next part of the algorithm uses this initial path along with actual front locations determined *in situ* by the AUV/ASV to adaptively generate subsequent waypoints for the AUV/ASV to track the frontal structure. Points on the velocity fronts are characterized by having near zero flow velocities. Therefore, while crossing a front, the micro-AUV is set up to detect periods where the measured flow velocity is below a specific threshold. The median point within this period is selected as the front location.

At the start, the AUV/ASV navigates along the initial zig-zag path generated based on the prior, until it detects two frontal crossings. Once two consecutive front locations, f_n and f_{n-1}, have been detected, the AUV/ASV estimates the next location of the front $\tilde{f}_{n+1}$, using a linear projection. In addition, once the front is crossed, the current destination waypoint p_n is recalculated to ensure that the vehicle does not travel too far beyond the front. The estimated front location and the current waypoint are then used to generate the next waypoint p_{n+1} for the AUV/ASV.

Algorithm 1: Adaptive Path generation

if $f_n isfound$ **then**
  $\tilde{f}_{n+1} = f_n + (f_n - f_{n-1}) \times a$
  $p_n = f_n + (f_n - p_{n-1}) \times b$
  $p_{n+1} = \tilde{f}_{n+1} + (\tilde{f}_{n+1} - p_n) \times c$
end if

In the algorithm, the constants a, b and c determine how far $\tilde{f}_{n+1}$, p_n and p_{n+1} are projected forward respectively. c needs to be set at a sufficiently large value to ensure that the sensing agent crosses the front in the next path segment. Even though this makes the next projected waypoint far away from the predicted front, it does not impact the performance of tracking strategy since this waypoint is recalculated when the next front location is detected.

We only utilize the first three waypoints of the initial path to initialize AUV/ASV on the front; the remaining waypoints are adaptively determined based on *in situ* data while tracking the time-varying front. The motivation for this method comes from the technique described in [4], which presents a front-following algorithm for remotely sensed data. Here, we attempt to adapt this heuristic based on static data into an adaptive planning algorithm that can be executed *in situ*. A detailed presentation of Algorithm 1, along with experimental results for Autonomous Surface Vehicles can be found in [8].

V. RESULTS

For each of the test scenarios presented in Section IV, multiple trials were run and the results were recorded. To evaluate the performance of the micro-AUV, as stated in previously, the initial parameters were the same as the ones used in [8].

Test 1: The final buoyancy was determined through *in situ* analysis and experimentation. After numerous trials, it was found that the seals and epoxy were successfully watertight, the structural integrity was confirmed for each part, and all components were fully-operational.

Test 2: The initial motor control parameters, as used in the mASV's in [8], induced heavy sway in the micro-AUV. With modifications to the controls program, a stable 2-D planar control was achieved. Given the size and speed of the micro-AUV, the associated Reynold's number is on the order of $10^4 - 10^5$, which is slightly lower than the vehicles the micro-AUV was modeled after. For comparison, the YSI EcoMapper AUV [47] and the Slocum Glider [48], which operate with a Reynold's number on the order of 10^6.

Test 3: With the micro-AUV being positively buoyant, a closed loop program used to define set waypoints for the micro-AUV was implemented, similar to the ASV used in [8]. The program successfully executed. The linear paths planned, as well as the path taken by the micro-AUV is shown in Fig. 6. While the vehicle was underwater, with the retro-reflective markers above water, the vehicle began the process around the point $(2.5, -1.8)$. It traversed the tank until reaching the starting waypoint at $(0.25, -1.6)$, and finishes just shy of the final waypoint at $(2.5, -2.3)$. Deviations from the path arise from a variety of sources. Poor calibration of the motion capture system occur where reflections on the water create inevitable dead zones. This is seen by low sampling spaces located around $(0.8, -1.5)$ and

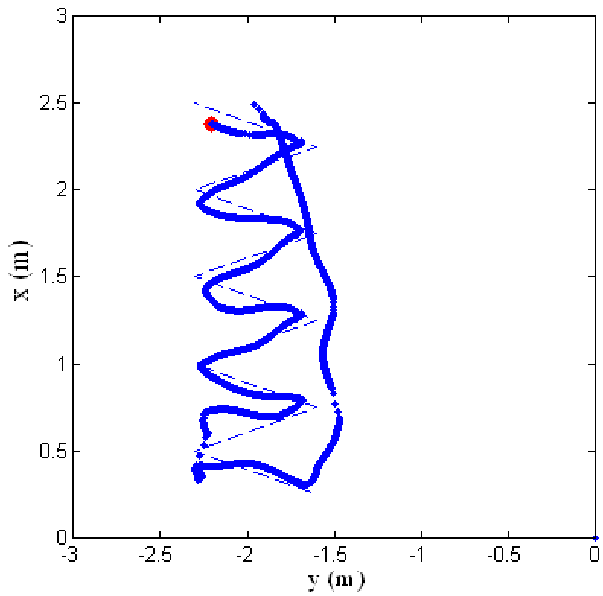

Fig. 6. Closed-loop program for reaching set way-points

$(0.5, -2.3)$. While the surface of the water is still, there are underwater circulations that are unaccountable in the mCoSTe. Likewise, the sway induced by forward motion cause the mico-AUV to sway slightly off path, and can cause over-corrections.

Test 4: Initially, the standard 2.4 GHz modules were tested and were discovered only to support reliable communication up to 0.17 m below the surface of the water. The next option to achieve communication through the entire 0.5 m of the tank was the 900 MHz XBee module. With the MR tank filled to $1/2$ depth, the 900 MHz XBee radio modules has a long enough wavelength and enough power to allow communication throughout the entire depth. As long as the markers stayed above water, tracking and localization was fully functional.

Test 5: Multiple underwater trials gave light to the limitations of the components used for pitch control, which only allowed a small pitch angle, less than $25°$. While successful 3-D motion was achieved, modification for greater pitch control is further discussed in Section VI.

Test 6: A flow field generated by (1) with parameters $A = 0.1$ and $\omega_b = \frac{1}{6\pi}$ was used in this experiment. Figure 7 shows the results when no measurement noise is considered. It can be observed that the front locations are detected very accurately in the absence of measurement noise. Similarly to the closed-loop program in **Test 3**, the micro-AUV experienced deviations while following the initial paths to the fixed waypoints. However, as the path was adaptively generated, taking into account the position and orientation of the vehicle, the generated paths were followed very well.

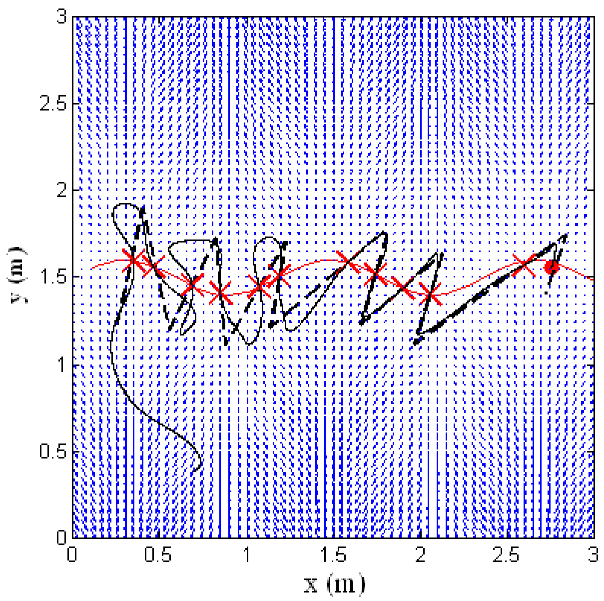

Fig. 7. Tracking a time-invariant velocity front in the absence of measurement noise

Test 7: The performance of the algorithm on time varying velocity fronts was tested using the flow field given by (2) with $A = 0.1$, $\omega_b = \frac{1}{6\pi}$ and $\omega_m = \frac{1}{\pi}$. Figure 8 shows the results of the tracking algorithm in the varying velocity flow field when the measurement noise was $I = 0.00$. Detection of the time-varying path was very successful in the absence of measurement noise, with all of the detection points being located within the swath of the front. Path deviations seen in **Test 7** are similar to those in **Test 6**. Immediately after each of the first 5 frontal detections, the micro-AUV experiences sway to the left. However, in both cases, after the adaptive path generation takes over these effects are mitigated.

Test 8: In this experiment, noise was added to the velocity measurements. The noisy measurements were low pass filtered using a Type II Chebyshev Filter before being used in the algorithm. This type of filter was used due to its low group delay. The result corresponding to a measurement noise of $I = 0.05$ is shown in Fig. 9. Contributing factors to error found include the measurement noise coupled with the path traveling in the same direction of the micro-AUV. This event initially registers the frontal velocity higher than the prescribed threshold, and slightly throws off the detection of the frontal boundary. Furthermore, while this trial had similar path deviations seen in **Test 6** and **Test 7**, they were also corrected after the 5^{th} detection.

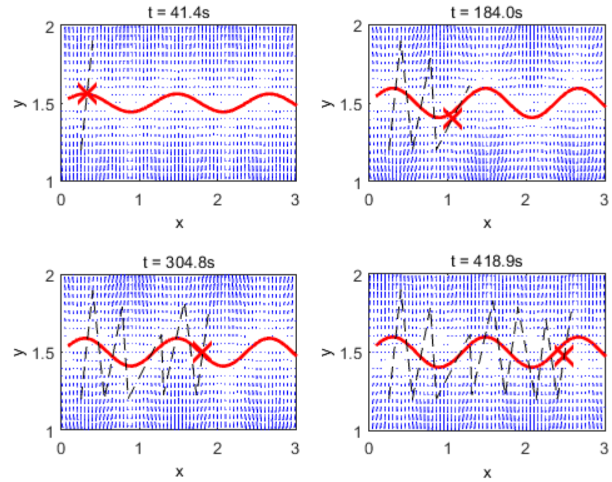

Fig. 8. Tracking a varying velocity front in the absence of measurement noise

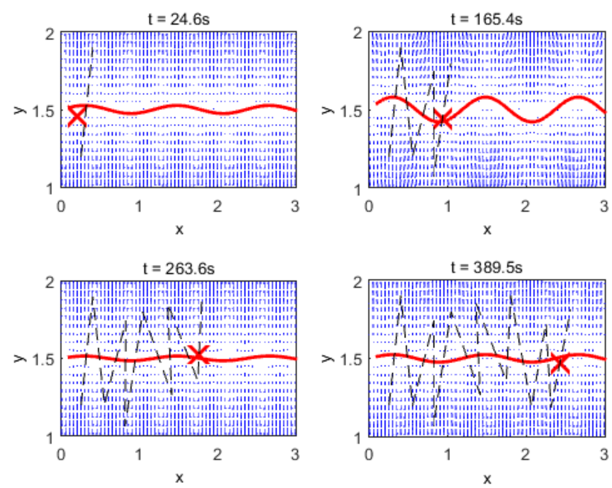

Fig. 9. Tracking a varying velocity front with measurement noise

VI. Conclusions and Future Work

In this paper we have developed and tested an autonomous vehicle that is able to track and sample spatiotemporally-varying coherent features in a laboratory aquatic environment. We have successfully tested and validated the vehicle in a variety of test cases where the algorithm designed in [8] was used to track a velocity front using a novel test-bed capable of creating controllable fluidic features in a laboratory setting. The main advantage of this vehicle is that we can test algorithms and strategies for 3-D sampling of dynamic ocean features in a laboratory environment.

Further development of the micro-AUV includes allocating yaw control solely to the rear propellers, which will lead to more accurate and efficient travel to way points, as well as adding two control planes to the right and left of the hull for stable and more precise control. Affixing the control planes to the bottom of the rear will help reduce the yaw and sway induced by momentum, allowing the motors to be throttled higher, which will lead to higher propulsion and quicker travel time. The increased speed of the micro-AUV will place it in a higher Reynold's number, around 10^6, similar to the vehicles that it was modeled after, and may help reduce measurement errors seen in **Test 8**. Altering the pitch control mechanism is desired by introducing dynamic buoyancy control that will double in function as buoyancy control and as pitch control. This will be located accordingly and will lead to finer depth movement resolution. We are also examining the integration of model predictions to inform the vehicle of frontal movements prior to starting the survey, or predicting frontal evolution during the execution of the mission. This will enable a longer horizon for path planning to place the vehicle in the *right place at the right time* to sample the entire front. Similar to [9], [10], the use of ocean model data for validation through simulations will aid in our progression to full scale field deployments, but also serves as a valuable intermediary for model testing in the mCoSTe. Additionally we aim to coordinate ASV and AUV to cooperatively sample dynamic features.

Acknowledgment

This work was supported by the Office of Naval Research (ONR) Award No. N000141310731. D. Heermance and R.N. Smith were partially supported by a Byron Dare Junior Faculty Award.

References

[1] Y. Zhang, M. A. Godin, J. G. Bellingham, and J. P. Ryan, "Using an Autonomous Underwater Vehicle to Track a Coastal Upwelling Front," *IEEE Journal of Oceanic Engineering*, vol. 37, pp. 338–347, July 2012.

[2] D. Olson, G. Hitchcock, A. Mariano, C. Ashjan, G. Peng, R. Nero, and G. Podesta, "Life on the edge: marine life and fronts," *Oceanography*, vol. 7, pp. 52–60, 1994.

[3] I. M. Belkin and J. E. O'Reilly, "An algorithm for oceanic front detection in chlorophyll and SST satellite imagery," *Journal of Marine Systems*, vol. 78, pp. 319–326, 2009.

[4] A. G. P. Shaw and R. Vennell, "A Front-Following Algorithm for AVHRR SST imagery," *Remote Sensing of Environment*, vol. 72, pp. 317–327, 2000.

[5] J. Hopkins, P. Challenor, and A. G. P. Shaw, "A new Statistical Modeling approach to ocean front detection from SST satellite images," *JTech*, vol. 27, pp. 173–191, 2010.

[6] G. Haller and G. Yuan, "Lagrangian coherent structures and mixing in two-dimensional turbulence," *Physica D: Nonlinear Phenomena*, vol. 147, pp. 352 – 370, Dec. 2000.

[7] R. N. Smith, P. Cooksey, F. Py, G. S. Sukhatme, and K. Rajan, "Adaptive Path Planning for Tracking Ocean Fronts with an Autonomous Underwater Vehicle," in *International Symposium on Experimental Robotics (ISER)*, (Marrakech and Essaouira, Morocco), pp. 1 —- 15, 2014.

[8] D. Kularatne, M. A. Hsieh, and R. N. Smith, "Zig-Zag Wanderer: Towards Adaptive Tracking of Time-Varying Coherent Structures in the Ocean," in *IEEE International Conference on Robotics and Automation*, (Seattle, WA), May 2015.

[9] B. Reed and F. Hover, "Oceanographic pursuit: Networked control of multiple vehicles tracking dynamic ocean features," *Methods in Oceanography*, pp. 1–23, May 2014.

[10] B. L. Reed and F. S. Hover, "Tracking ocean fronts with multiple vehicles and mixed communication losses," in *Intelligent Robots and Systems (IROS), 2013 IEEE/RSJ International Conference on*, pp. 3374–3381, Nov. 2013.

[11] J. Yuh, "Design and Control of Autonomous Underwater Robots: A Survey," *Autonomous Robots*, vol. 8, pp. 7–24, 2000.

[12] D. A. Paley, F. Zhang, and N. E. Leonard, "Cooperative Control for Ocean Sampling: The Glider Coordinated Control System," *IEEE Transactions on Control Systems Technology*, vol. 16, pp. 735–744, July 2008.

[13] R. N. Smith, M. Schwager, S. L. Smith, B. H. Jones, D. Rus, and G. S. Sukhatme, "Persistent Ocean Monitoring with Underwater Gliders: Adapting Sampling Resolution," *Journal of Field Robotics*, vol. 28, no. 5, pp. 714–741, 2011.

[14] R. N. Smith, J. Das, H. Heidarsson, A. Pereira, I. Cetinić, L. Darjany, M.-E. Garneau, M. D. Howard, C. Oberg, M. Ragan, A. Schnetzer, E. Seubert, E. C. Smith, B. A. Stauffer, G. Toro-Farmer, D. A. Caron, B. H. Jones, and G. S. Sukhatme, "{USC} {CINAPS} Builds Bridges: Observing and Monitoring the {S}outhern {C}alifornia {B}ight," *IEEE Robotics and Automation Magazine, Special Issue on Marine Robotics Systems*, vol. 17, pp. 20–30, Mar. 2010.

[15] R. N. Smith, Y. Chao, P. P. Li, D. A. Caron, B. H. Jones, and G. S. Sukhatme, "Planning and Implementing Trajectories for Autonomous Underwater Vehicles to Track Evolving Ocean Processes based on Predictions from a Regional Ocean Model," *International Journal of Robotics Research*, vol. 29, pp. 1475–1497, Oct. 2010.

[16] R. N. Smith, A. Pereira, P. P. Li, D. A. Caron, B. H. Jones, and G. S. Sukhatme, "Autonomous Underwater Vehicle trajectory design coupled with predictive ocean models: A case study," in *2010 IEEE International Conference on Robotics and Automation*, pp. 4770–4777, IEEE, 2010.

[17] E. L. Creed, C. Mudgal, S. Glenn, O. Schofield, C. Jones, and D. C. Webb, "Using a Fleet of Slocum Battery Gliders in a Regional Scale Coastal Ocean Observatory," in *Oceans '02 MTS/IEEE*, 2002.

[18] A. Garcia-Olaya, F. Py, J. Das, and K. Rajan, "An Online Utility-Based Approach for Sampling Dynamic Ocean Fields," *IEEE Journal of Oceanic Engineering*, vol. 37, pp. 185–203, Apr. 2012.

[19] H. Singh, D. Yoerger, and A. Bradley, "Issues in AUV Design and Deployment for Oceanographic Research," in *Proceedings of the 1997 IEEE International Conference on Robotics and Automation*, vol. 3, pp. 1857–1862, 1997.

[20] E. Fiorelli, N. E. Leonard, P. Bhatta, D. A. Paley, R. Bachmayer, and D. M. Fratantoni, "Multi-AUV Control and Adaptive Sampling in Monterey Bay," *Oceanic Engineering, IEEE Journal of*, vol. 31, pp. 935–948, Oct. 2006.

[21] Y. Zhang, M. Godin, J. G. Bellingham, and J. P. Ryan, "Ocean front detection and tracking by an autonomous underwater vehicle," in *MTS/IEEE Oceans 2011*, pp. 1–4, Sept. 2011.

[22] Y. Zhang, J. G. Bellingham, J. P. Ryan, B. Kieft, and M. J. Stanway, "Two-dimensional mapping and tracking of a coastal upwelling front by an autonomous underwater vehicle," in *MTS/IEEE Oceans - San Diego*, pp. 1–4, Sept. 2013.

[23] I. M. Belkin, P. C. Cornillon, and K. Sherman, "Fronts in Large Marine Ecosystems," *Progress In Oceanography*, vol. 81, no. 1-4, pp. 223–236, 2009.

[24] J. Hopkins, P. Challenor, and A. G. P. Shaw, "A New Statistical Modeling Approach to Ocean Front Detection from SST Satellite Images," *Journal of Atmospheric and Oceanic Technology*, vol. 27, pp. 173–191, Jan. 2010.

[25] B. Zhang and G. S. Sukhatme, "Adaptive Sampling With Multiple Mobile Robots," in *IEEE International Conference on Robotics and Automation (submitted)*, 2008.

[26] N. E. Leonard, D. A. Paley, R. E. Davis, D. M. Fratantoni, F. Lekien, and F. Zhang, "Coordinated control of an underwater glider fleet in an adaptive ocean sampling field experiment

in Monterey Bay," *Journal of Field Robotics*, vol. 27, no. 6, pp. 718–740, 2010.

[27] J. Das, T. Maughan, M. McCann, M. Godin, T. O'Reilly, M. Messie, F. Bahr, K. Gomes, F. Py, J. Bellingham, G. Sukhatme, and K. Rajan, "Towards mixed-initiative, multi-robot field experiments: Design, deployment, and lessons learned," in *Proceedings of the Intelligent Robots and Systems (IROS) Conference*, (San Francisco), 2011.

[28] K. Gomes, D. Cline, D. Edgington, M. Godin, T. Maughan, M. McCann, T. O'Reilly, F. Bahr, F. Chavez, M. Messi, J. Das, and K. Rajan, "{ODSS}: A Decision Support System for Ocean Exploration," in *Workshop on Data-Driven Decision Guidance and Support Systems (DGSS) at the 29th IEEE International Conference on Data Engineering*, (Brisbane, Australia), 2013.

[29] G. A. Hollinger and G. S. Sukhatme, "Trajectory Learning for Human-robot Scientific Data Collection," in *IEEE International Conference on Robotics and Automation*, no. Section V, (Hong Kong), pp. 1–6, May 2014.

[30] B. Garau, A. Alvarez, and G. Oliver, "Path Planning of Autonomous Underwater Vehicles in Current Fields with Complex Spatial Variability: an {A}* Approach," in *Proceedings of the IEEE International Conference on Robotics and Automation*, (Barcelona, Spain), 2005.

[31] A. Zamuda and D. Hernández, "Differential Evolution and Underwater Glider Path Planning Applied to the Short-Term Opportunistic Sampling of Dynamic Mesoscale Ocean Structures," *Applied Soft Computing*, vol. 24, pp. 95 – 108, 2014.

[32] C. Hsieh, Z. Jin, D. Marthaler, B. Nguyen, D. Tung, A. Bertozzi, and R. Murray, "Experimental validation of an algorithm for cooperative boundary tracking," in *American Control Conference*, pp. 1078–1083, 2005.

[33] S. Susca, S. Martinez, and F. Bullo, "Monitoring environmental boundaries with a robotic sensor network," *IEEE Transactions on Control Systems Technology*, vol. 16, no. 2, pp. 288 – 296, 2008.

[34] I. Triandaf and I. B. Schwartz, "A collective motion algorithm for tracking time-dependent boundaries," *Mathematics and Computers in Simulation*, vol. 70, pp. 187 – 202, 2005.

[35] V. M. Goncalves, L. C. A. Pimenta, C. A. Maia, B. Dutra, and G. A. S. Pereira, "Vector fields for robot navigation along time-varying curves in n-dimensions," *IEEE Transactions on Robotics*, vol. 26, no. 4, pp. 647 – 659, 2010.

[36] F. Zhang, D. M. Fratantoni, D. Paley, J. Lund, and N. E. Leonard, "Control of coordinated patterns for ocean sampling," *International Journal of Control*, vol. 80, no. 7, pp. 1186 – 1199, 2007.

[37] K. M. Lynch, I. B. Schwartz, P. Yang, and R. A. Freeman, "Decentralized Environmental Modeling by Mobile Sensor Networks," *IEEE Transactions on Robotics*, vol. 24, pp. 710–724, June 2008.

[38] W. Wu and F. Zhang, "Cooperative exploration of level surfaces of three dimensional scalar fields," *Automatica*, vol. 47, pp. 2044–2051, Sept. 2011.

[39] M. Michini, M. A. Hsieh, E. Forgoston, and I. B. Schwartz, "Robotic tracking of coherent structures in flows," *IEEE Transactions on Robotics*, vol. 30, no. 3, pp. 593–603, 2014.

[40] Micromo, "Dcmotors," *http://www.micromo.com/*.

[41] D. Larkin, M. Michini, A. Abad, S. Teleski, and M. A. Hsieh, "Design of the multi-robot coherent structure testbed (mcoste) for distributed tracking of geophysical fluid dynamics." 2014.

[42] Sparkfun, "Nanoservo," *https://www.sparkfun.com/products/11882*.

[43] Sparkfun, "microbattery," *https://www.sparkfun.com/products/339*.

[44] Sparkfun, "900xbee," *https://www.sparkfun.com/products/11634*.

[45] M. Michini, K. Mallory, D. Larkin, M. A. Hsieh, E. Forgoston, and P. A. Yecko, "An experimental testbed for multi-robot tracking of manifolds and coherent structures in flows." 2013.

[46] G. Veronis, "Wind-driven oceans circulation, part i and part ii," *Deep Sea Res.*, vol. 13, no. 31, 196.

[47] {YSI} Incorporated, "YSI EcoMapper - http://www.ysi.com/productsdetail.php?EcoMapper-41," 2015.

[48] O. Schofield, J. Kohut, D. Aragon, E. L. Creed, J. G. Graver, C. Haldman, J. Kerfoot, H. Roarty, C. Jones, D. C. Webb, and S. Glenn, "Slocum gliders: Robust and ready," *Journal of Field Robotics*, vol. 24, no. 6, pp. 473–485, 2007.